Speed Control for Robust Path-Tracking for Automated Vehicles at the Tire-Road Friction Limit

Vincent A. Laurense & J. Christian Gerdes
Department of Mechanical Engineering
Stanford University, Stanford, United States
E-mail: laurense@stanford.edu

Topics / Vehicle Automation and Connection, Vehicle Dynamics and Chassis Control

July 11, 2018

At the limit of tire-road friction, steering becomes an ineffective control input for tracking a desired path. In challenging automated driving scenarios, conventional lateral control through steering could therefore lead to road departures or hinder successful evasive maneuvers. Conservative path planning might prevent the occurrence of uncontrollable path-tracking dynamics; however, not using the full tire-force potential can also impede a successful emergency maneuver. This paper presents a novel control framework for consistent and full tire-force utilization with slip-angle based steering control, combined with explicit control of the path-tracking dynamics through longitudinal speed feedback. Experimental results with a full-scale automated race car demonstrate the framework achieving path tracking with consistent tire-force utilization, even when the estimate of available tire-road friction is inaccurate, while a conventional control architecture either underutilizes the tire-force potential, or slides off the path when friction is overestimated.

1 INTRODUCTION

Conventional control architectures for automated vehicles employ independent lateral and longitudinal control [1]–[3]. Given the geometry of a desired path and an estimate of the local tire-road friction coefficient, a speed profile can be computed that should always keep the tire forces within their physical limits, for example for a planar road as described by Kritayakirana [2] and for a path with 3D topography by Subosits and Gerdes [4]. This is important for planning and executing emergency maneuvers that can use the full tire-force potential. Estimation of the maximum forces that a tire can generate, however, requires accurate estimates of the local tire-road friction coefficient and the tire's normal load, which are difficult to obtain in real-time [5].

More importantly, while aiming to drive at the physical limit in a critical maneuver, any amount of excessive speed due to overestimation of the friction coefficient or normal load, or failure to closely track the safe speed profile, directly leads to full saturation of the tires and the loss of control of the path-tracking states. This could lead to significant deviations from an obstacle-free desired path and even road departures. Conservative approaches to prevent tire-force saturation and the associated loss of path-tracking control, on the other hand, could lead to underutilization of the tire-force potential, which in turn limits the vehicle's capability to successfully execute the maneuver.

As noted by Laurense *et al.* [5], the seemingly conflicting objectives of path tracking while consistently cornering at the limit of friction could be addressed by a control framework that employs slip-angle based steering control to robustly operate the tires at their peak force, while speed feedback controls the path-tracking states. This approach bears similarity with limit vehicle handling portrayed by a professional race car driver, and inherently provides robustness against uncertainty and variations in the tire-road friction coefficient.

This paper presents a novel control framework with speed feedback for path tracking, in conjunction with a slip-angle based steering controller developed by Subosits and Gerdes [6]. The framework leverages the center of percussion to develop a path-tracking controller for a limit-understeering vehicle, without the need for a model of the lateral forces at the rear axle.

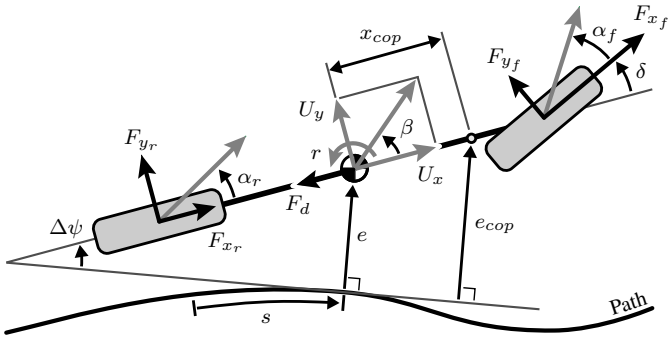

Figure 1: Planar single-track vehicle model

After an analytical analysis of their closed-loop behavior, the path-tracking performance of the new design is compared experimentally to a conventional control architecture with steering control for path tracking and independent longitudinal control designed for operating the tires at their limits. The experiment, with a full-scale automated race car, considers a range of *a priori* tire-road friction coefficient estimates to explicitly investigate the robustness of the two approaches, and their ability to consistently use the true full tire-force potential.

2 MODELING

2.1 Vehicle Model

The planar single-track vehicle model in Fig. 1 has three velocity states related to its center of gravity (CG): longitudinal speed U_x and lateral speed U_y – together establishing side slip β – and yaw rate r. Furthermore, there are three position states in relation to a desired path: the distance along this path and the lateral distance, s and e, respectively, and the difference in heading between the vehicle and the path, denoted by $\Delta\psi$. The path is described by curvature $\kappa(s)$. Drag forces, e.g. aerodynamic drag and rolling resistance, are represented by F_d. The vehicle has mass m and yaw moment of inertia I_{zz}. The distance from the CG to the front and rear axle is denoted by a and b, respectively, summing up to the wheelbase L. The front steer angle is indicated by δ.

Table 1: Vehicle & tire model parameters

Parameter	Value	Symbol	Unit
Vehicle mass	m	1,659	kg
Yaw moment of inertia	I_{zz}	2,400	kg $\cdot$ m^2
Distance front axle to CG	a	1.015	m
Distance rear axle to CG	b	1.453	m
Front cornering stiffness	C_{α_f}	225	kN/rad
Rear cornering stiffness	C_{α_r}	250	kN/rad
Front friction coefficient	μ_f	0.99	-
Rear friction coefficient	μ_r	1.04	-

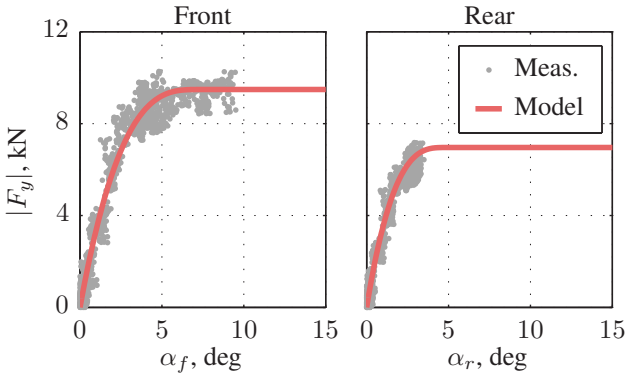

Figure 2: Measured and modeled lateral forces at the front (left) and rear (right) axle in a rampsteer maneuver

The system is governed by nonlinear equations of motion:

$$\dot{U}_x = \frac{-F_{y_f}\sin\delta + F_{x_f}\cos\delta + F_{x_r} - F_d}{m} + rU_y \tag{1a}$$

$$\dot{U}_y = \frac{F_{y_f}\cos\delta + F_{x_f}\sin\delta + F_{y_r}}{m} - rU_x \tag{1b}$$

$$\dot{r} = \frac{a\left(F_{y_f}\cos\delta + F_{x_f}\sin\delta\right) - bF_{y_r}}{I_{zz}} \tag{1c}$$

$$\dot{s} = \frac{U_x\cos\Delta\psi - U_y\sin\Delta\psi}{1-\kappa e} \tag{1d}$$

$$\dot{e} = U_x\sin\Delta\psi + U_y\cos\Delta\psi \tag{1e}$$

$$\Delta\dot{\psi} = r - \kappa\dot{s}. \tag{1f}$$

Table 1 lists the parameters for an Audi TTS research vehicle.

2.2 Tire Model

For modeling the lateral force of the lumped tires at each of the axles in the single-track model, a Fiala brush model with a single tire-road friction coefficient is used [7]. This model describes the lateral tire force as a function of slip angle α, cornering stiffness C_α, normal load F_z and tire-road friction coefficient μ, with:

$$F_y = \begin{cases} -C_\alpha\tan\alpha + \frac{C_\alpha^2}{3\mu F_z}|\tan\alpha|\tan\alpha \\ \quad -\frac{C_\alpha^3}{27\mu^2F_z^2}\tan^3\alpha & \text{if } |\alpha| < \alpha_{sl}, \\ -\mu F_z\,\mathrm{sgn}\,\alpha & \text{otherwise,} \end{cases} \tag{2}$$

where α_{sl} is the peak slip angle at which total sliding occurs:

$$\alpha_{sl} = \arctan\left(\frac{3\mu F_z}{C_\alpha}\right). \tag{3}$$

With this model the full lateral force potential is reached at α_{sl}.

Figure 2 depicts the lateral forces measured in a quasi-steady state rampsteer maneuver, using (1b) and (1c) with steady-state assumptions, measurements of U_x, U_y and r, and assuming $\delta \approx 0$. The plot overlays the lateral forces modeled by the brush model, for which the parameters are included in Table 1.

3 PATH TRACKING AT THE FRICTION LIMIT

A typical car portrays limit-understeer behavior, which means that in steady-state cornering the front tires will saturate before the rear tires. For such a vehicle the capability to control the path-tracking dynamics with the steering wheel disappears as soon as the front tires are saturated. To see this, consider a linearization of the front tire in the single-track vehicle model at constant longitudinal speed. Differentiation of (2) with respect to slip angle yields local cornering stiffness C_f at the front axle, which goes from C_{α_f} at zero slip to zero at the peak slip angle. The linearization describes the front lateral force in response to a change in the front slip angle, which is a function of the steer angle:

$$F_{y_f} \approx F_{y_{f_0}} + \left.\frac{\partial F_y}{\partial\alpha_f}\right|_0\tilde{\alpha}_f \tag{4a}$$

$$\approx F_{y_{f_0}} - C_f\left(\frac{\tilde{U}_y + a\tilde{r}}{U_x} - \tilde{\delta}\right), \tag{4b}$$

where a tilde over a variable indicates its deviation from the linearization condition. Equation 4b illustrates that when the front tires are fully saturated, i.e. when $C_f = 0$, steering has no effect on the front lateral force. This means that when the front tires are operating at their peak slip angle and generating their maximum amount of lateral force, steering is no longer an input that can be used for controlling the path-tracking dynamics.

An analysis of the closed-loop poles of the linearized system provides more insight in the path-tracking behavior of an automated vehicle as it is approaching tire-force saturation. The equations of motion in (1f) are linearized around the equilibrium conditions and the desired path, i.e. $e = 0$ and $\Delta\psi = 0$. Furthermore, it is assumed that the longitudinal tire forces, drag force and the steer angle are zero. In the analysis a range of equilibrium conditions is considered, selected by sweeping C_f in (4b) from C_{α_f} to zero, i.e. from zero to full front tire-force saturation. The corresponding rear local cornering stiffness C_r is found with the force balance in steady-state conditions, i.e. $F_{y_{r0}} = {}^a\!/_b\, F_{y_{f_0}}$, and inversion of (2) yields the rear slip angle around which the rear tire model is linearized.

In a conventional control architecture with an independent lateral control module with steering for tracking a desired path, e.g. the center of a lane or the racing line on a race track, one could employ a simple lane-keeping controller [8]. This provides steering feedback based on the look-ahead error e_{LA}, which is the projected lateral error at a distance x_l ahead of the CG:

$$\delta_{FB} = -k_l e_{LA} = -k_l\left(e + x_l\sin\left(\Delta\psi - \beta_{ss}\right)\right). \tag{5}$$

Kapania and Gerdes describe this controller in more detail in [8].

The resulting dynamics of the closed-loop linearized system can then be written as:

$$\dot{\tilde{x}} = A\tilde{x} + B\kappa, \tag{6}$$

where $x = [U_y\ r\ e\ \Delta\psi]^T$ and

$$A = \begin{bmatrix} \frac{-\tilde{C}_f-\tilde{C}_r}{mU_x} & \frac{b\tilde{C}_r-a\tilde{C}_f}{mU_x} - U_x & \frac{-\tilde{C}_f k_l}{m} & \frac{-\tilde{C}_f k_l x_l}{m} \\ \frac{b\tilde{C}_r-a\tilde{C}_f}{I_{zz}U_x} & \frac{-\left(a^2\tilde{C}_f+b^2\tilde{C}_r\right)}{I_{zz}U_x} & \frac{-a\tilde{C}_f k_l}{I_{zz}} & \frac{-a\tilde{C}_f k_l x_l}{I_{zz}} \\ 1 & 0 & 0 & U_x \\ 0 & 1 & -U_x\kappa^2 & 0 \end{bmatrix}. \tag{7}$$

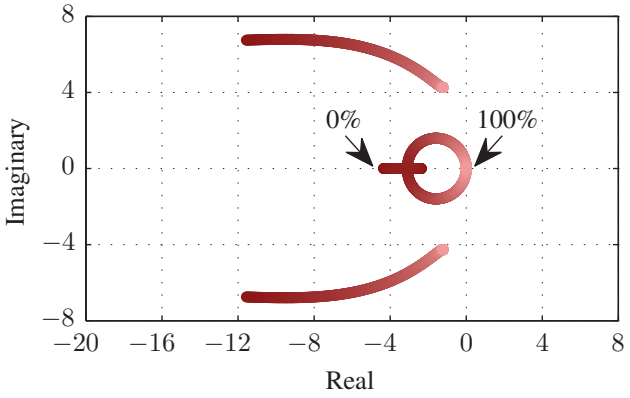

Figure 3: Poles of the closed-loop system in (7) for $k_l = 0.0538$ rad/m, $x_l = 14.21$ m and $\kappa = 0$ at $U_x = 20$ m/s, with the linearizations from 0% to 100% front lateral force

Figure 3 shows how the poles of this closed-loop system move in the complex plane as the front lateral force is swept from zero to full saturation. At full tire-force saturation, the slower poles arrive at the origin. The marginally stable characteristics of those integrators describe how the vehicle will slide away from the desired path when the front tires are at their saturation limits.

4 CONTROLLER DESIGN

4.1 Speed Control

Section 3 illustrates that when a limit-understeering vehicle is operated at maximum front lateral force, steering is no longer an input that can control the path-tracking states. Starting with an analysis of the dynamics of a unique point on the vehicle's centerline, the center of percussion (COP), it is shown how longitudinal speed can be used as an input to control the path-tracking states instead.

Milliken *et al.* introduce the COP, which can be interpreted as the location along the vehicle's centerline at which no lateral reaction force is experienced in response to a lateral force at the rear axle [9]. It is the point where the effect of a lateral force at the rear axle on the lateral acceleration is canceled by the effect on the rotational acceleration. Kritayakirana leverages the COP for the design of a steering controller [2]; in particular the projected error of the COP to a desired path, which is the combination of the lateral error at the CG and the heading error:

$$e_{cop} = e + x_{cop} \sin \Delta\psi, \tag{8}$$

where x_{cop} is the distance from the CG to the COP, as depicted in Fig. 1. The advantage of using the COP in this context, and not any other point along the vehicle's centerline, is that the dynamics of the projected error at this point do not depend on the rear lateral force F_{y_r}:

$$\ddot{e}_{cop} = \frac{L}{b}\frac{F_{y_f}}{m} - U_x \kappa \dot{s} - x_{cop}\left(\kappa \ddot{s} + \dot{\kappa}\dot{s}\right). \tag{9}$$

This expression describes how in normal driving scenarios conventional lateral control through steering can control the path-tracking states with front lateral force F_{y_f}. It also shows that the vehicle's path-tracking dynamics become uncontrolled when the front lateral force F_{y_f} saturates. In fact, at this point the path-tracking dynamics are ballistic due to an imbalance between the available and the required centripetal acceleration to stay on the desired path.

Nonetheless, (9) does reveal two options to prevent uncontrollable growth of the projected error in that case: decrease the curvature of the desired path to track a different, feasible, trajectory; or reduce the vehicle's speed in order to reduce the centripetal acceleration required to stay on the original path – this paper focuses on the latter.

With an estimate of the tire-road friction coefficient, a vehicle model and the desired path that is to be tracked, a maximum permissible speed profile can be designed with the goal to keep the tire forces within their physical limits [2], [4]. The proposed framework aims to leverage this speed profile, through which the vehicle can anticipate upcoming turns and can account for the 3D topography of the desired path, and use longitudinal speed feedback on top of that to robustly control the path-tracking states in the turns, even when steering is no longer effective.

For the derivation of this concept, consider imposing stable second-order dynamics to drive the projected error at the COP to zero, with bandwidth ω_n and damping ζ:

$$\ddot{e}_{cop} + 2\zeta\omega_n \dot{e}_{cop} + \omega_n^2 e_{cop} = 0. \tag{10}$$

Assuming that the third term in (9) is negligible with respect to the first two and that the car remains relatively close to the path such that (1d) can be simplified to $\dot{s} \approx U_x$, substitution of (9) into (10) and solving for U_x leads to the following longitudinal speed command;

$$\bar{U}_x = \sqrt{\frac{\frac{\hat{F}_{y_f} L}{mb} + 2\zeta\omega_n \dot{e}_{cop} + \omega_n^2 e_{cop}}{\kappa}} \quad \text{for } \kappa \neq 0. \tag{11}$$

In this expression $\hat{F}_{y_f}$ denotes the modeled front lateral force that is consistent with the current slip-angle command, and is computed according to the nonlinear model in (2). It is assumed that the longitudinal tire forces for making minor speed corrections do not affect the front lateral force capability significantly, and that the front axle normal load follows from the vehicle's static weight distribution. The friction estimate can come from an online friction estimator, or can be an *a priori* estimate.

Next, a speed controller is designed by filtering the speed command, with a first-order filter with a stable pole at k_f:

$$\dot{\bar{U}}_{x_f} + k_f \bar{U}_{x_f} = k_f \bar{U}_x, \tag{12}$$

followed by imposing stable first-order dynamics on the filtered speed error, for which the pole is at k_u:

$$\dot{\bar{U}}_{x_f} - \dot{U}_x = -k_u\left(\bar{U}_{x_f} - U_x\right). \tag{13}$$

For small steer angles (1a) yields:

$$F_x - F_d \approx m\dot{U}_x. \tag{14}$$

This leads to the following longitudinal force command, which achieves the desired path-tracking dynamics in (10) through control of the vehicle's longitudinal speed according to (11):

$$F_x = mk_u\left(\bar{U}_{x_f} - U_x\right) + m\dot{\bar{U}}_{x_f} + F_d. \tag{15}$$

This concept can now easily be extended to work on top of a pre-computed speed profile, by calculating a speed correction term that will only respond to path-tracking errors:

$$\Delta\bar{U}_x = \sqrt{\frac{\frac{\hat{F}_{y_f} L}{mb} + 2\zeta\omega_n \dot{e}_{cop} + \omega_n^2 e_{cop}}{\kappa}} - \sqrt{\frac{\frac{\hat{F}_{y_f} L}{mb}}{\kappa}}. \tag{16}$$

This term is added to the longitudinal speed command $\bar{U}_x^P$ that follows from the speed profile, to finally obtain:

$$F_x = mk_u\left(\bar{U}_x^P + \Delta\bar{U}_{x_f} - U_x\right) + m\left(\dot{\bar{U}}_x^P + \Delta\dot{\bar{U}}_{x_f}\right) + F_d. \tag{17}$$

This framework leverages the pre-computed speed profile, with its 3D topography model and its capability to anticipate upcoming turns. The vehicle's speed is seamlessly adjusted to control the path-tracking states with only relatively simple models of horizontal path curvature and front lateral force, even when steering is no longer an effective input.

In this control design, there are four tuning parameters:

- Path-tracking dynamics: ω_n & ζ
- Speed command filter pole: k_f
- Speed error dynamics pole: k_u

Ideally, the speed command filter pole k_f and the pole for the imposed speed error dynamics k_u are significantly faster than the poles for the imposed path-tracking dynamics (resulting from ω_n and ζ), while the bandwidth of the latter is high enough to achieve satisfactory path-tracking performance and the imposed speed-tracking dynamics respect the engine limitations.

4.2 Slip-Angle Control

4.2.1 *Stability of Slip-Angle vs. Steer-Angle Tracking*

To maximize the cornering capability of a limit-understeering vehicle, a straightforward approach would seem to always operate the front tires at their peak slip angle. This, however, leads to poor stability properties.

Consider maintaining a fixed front slip angle, which could be any slip angle between zero and the peak slip angle at which full saturation occurs. This means that the front lateral force is fixed; only the rear lateral force changes in response to deviations from the equilibrium condition. The linearized equations of motion for the vehicle's lateral velocity and yaw rate, respectively, yields the following state matrix:

$$\tilde{A}_\alpha = \begin{bmatrix} \frac{-\tilde{C}_r}{mU_x} & \frac{b\tilde{C}_r}{mU_x} - U_x \\ \frac{b\tilde{C}_r}{I_{zz}U_x} & \frac{-b^2\tilde{C}_r}{I_{zz}U_x} \end{bmatrix}. \tag{18}$$

In contract, consider the scenario in which the steering angle of the vehicle is held constant. The linearized front axle lateral force in the single-track model in that case is given by:

$$F_{y_f} \approx F_{y_{f_0}} - \tilde{C}_f \left(\frac{\tilde{U}_y + a\tilde{r}}{U_x} \right). \tag{19}$$

Substituting this in the linearized equations of motion yields the following state matrix:

$$\tilde{A}_\delta = \begin{bmatrix} \frac{-\tilde{C}_f - \tilde{C}_r}{mU_x} & \frac{b\tilde{C}_r - a\tilde{C}_f}{mU_x} - U_x \\ \frac{b\tilde{C}_r - a\tilde{C}_f}{I_{zz}U_x} & \frac{-\left(a^2\tilde{C}_f + b^2\tilde{C}_r\right)}{I_{zz}U_x} \end{bmatrix}. \tag{20}$$

Figure 4 depicts the closed-loop poles of these systems, with either the steer angle or the slip angle held constant. As expected, the poles end up in the same location, where the front tires are fully saturated and $C_f = 0$. Before saturation, however, the system in which the steer angle is fixed has superior damping characteristics over the system in which the front slip angle is fixed.

4.2.2 *Feedforward and Feedback Steering*

The lateral controller for the proposed framework is designed with two requirements: while aiming to corner at the limit it should use the full front tire-force potential consistently, and the controller should portray good damping characteristics while approaching the tire-road friction limit.

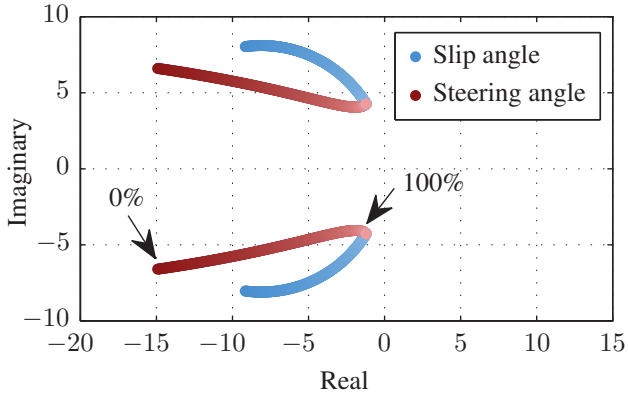

Figure 4: Closed-loop poles of the lateral vehicle dynamics at $U_x = 20$ m/s with either steer angle or front slip angle fixed with the linearizations from 0% to 100% front lateral force

Subosits and Gerdes designed a high performance slip-angle based lateral controller [6], which lends itself well for the proposed framework. This controller tracks a front slip-angle command $\bar{\alpha}_f$, which combines a feedforward and a feedback term:

$$\bar{\alpha}_f = \alpha_{FF} + \alpha_{FB}, \tag{21}$$

where

$$\alpha_{FB} = -\delta_{FB} + \arctan\frac{U_y + ar}{U_x} - \arctan\frac{U_y + ar}{U_x}\bigg|_{FF}. \tag{22}$$

In this design δ_{FB} is the steering feedback term that results from the look-ahead error, as in (5). The latter two terms make this slip-angle based controller equivalent to a steer-angle based controller, leveraging its favorable stability characteristics. More details on this controller can be found in the appendix in [6].

To make the vehicle corner consistently at the limit of tire-road friction and use its full front tire-force potential, the feedforward slip angle α_{FF} is set to the front peak slip angle that is computed from (3). When the vehicle is traveling slower than intended, or the tire-road friction coefficient is higher than anticipated, the vehicle will then still use virtually all available friction [5], as it starts to make a turn that is tighter than the desired path. This is not a problem, however, as the speed controller will continuously drive the vehicle back to the path according to the imposed path-tracking dynamics. To make the new framework function in all conditions, including straights, the feedforward slip angle is computed from the lateral forces that the pre-computed speed profile demands, by inverting (2). In pure cornering conditions the speed profile will require all available front lateral force and thus demand peak slip angle, as desired.

While steering feedback is required to control the path-tracking states on straight sections, in the turns only speed feedback, not steering feedback, is desired to make sure the front tires are operated at their very limit. Namely, when the car is on the inside of the turn it should speed up rather than sacrificing slip angle – i.e. tire-force utilization – by steering out towards the path. Vice versa the car should not try to turn in more when it finds itself on the outside of the path, since the front tires are already saturated.

Discrete steps in the commanded slip angle, that would result from switching slip-angle feedback off in the turns, however, are undesirable, since these could inject a strong disturbance into the vehicle's dynamics. Therefore, a variable dead band is computed for the look-ahead error e_{LA}. The dead band, which is computed offline, is ramped in when the desired lateral acceleration is more than 70% of the maximum lateral acceleration, and the ramp-in rate is selected such that the resulting steering rate at the hand wheel is limited to 45 deg/s. This scheme maintains steering feedback on the straights, leads to smooth steering inputs, and could in addition provide a safety mechanism to steer out of a turn in case speed feedback alone is not sufficient.

Figure 5: Automated 2009 Audi TTS Quattro research vehicle

Note that the framework does not require the front axle to always be operated at its very limit. The framework also works when a fraction of the available tire forces is to be used, as long as the feedforward front slip angle is computed accordingly. Only when the speed profile dictates the car to use *all* available friction will the front tires be operated at their peak slip angle.

5 EXPERIMENTAL SETUP

The proposed integrated framework is tested on the full-scale automated vehicle depicted in Fig. 5, and compared to a conventional control framework with a lane-keeping steering controller for path tracking and decoupled longitudinal control [2]. The proposed framework is configured with $\omega_n = 1$ rad/s, $\zeta = 0.4$, $k_f = 1.5$ rad/s and $k_u = 2.5$ rad/s. The testbed is equipped with electronic power steering, a controllable brake booster, throttle-by-wire, a direct-shift gearbox (DSG), a controller area network (CAN) interface to obtain vehicle data and Bridgestone Potenza S-04 tires. The controllers run at 200 Hz on a dSPACE MicroAutoBox II, and a dual antenna OxTS RT4003 integrated inertial navigation system (INS) with differential global positioning system (dGPS) operating at 250 Hz measures the vehicle and path-tracking states.

The experiment takes place in turn 2 at Thunderhill Raceway Park in Willows, CA, which is a long 180 deg left-hand turn. The desired path has a constant curvature for this turn with $\kappa \approx 0.011$ m^{-1}. The *a priori* estimates of the tire-road friction coefficient $\hat{\mu}$ are varied from 0.86 to 0.99; in dry conditions the true friction coefficient is approximately 0.95. It is hypothesized that the new framework consistently uses the tire-force potential, while the conventional architecture is expected to underutilize the tire-force potential when friction is underestimated, and to slide off the path when friction is overestimated.

6 RESULTS

Figure 6a shows that with the conventional controller and relatively low friction estimates – which underestimate the tire-force potential – the car can track the desired path, i.e. the path-tracking error is not growing. Starting at $\hat{\mu} = 0.96$, however, it can no longer always follow the desired path – the car is sliding towards the outside of the turn despite increasing the front slip angle, as depicted in Fig. 6b. The longitudinal speed plotted in Fig. 6c behaves as expected: with higher friction estimates the vehicles tries to track a faster speed profile, and is able to do so when the friction estimates and the resulting desired speed are relatively low. When friction is overestimated, however, the vehicle actually loses longitudinal speed towards the end of the turn, as the large steering angle causes significant drag.

In contrast, with speed feedback the car never slides away from the path uncontrollably: Fig. 6a shows that the car is never more than 1 m off the path, even with overly optimistic *a priori* friction estimates that would cause the conventional steering controller to slide off the path more than 2 m. Figure 7 also illustrates how the driven trajectories are relatively close together, i.e. close to the desired path. With the new framework the front tires are operated consistently at a slip angle of approximately -6 deg, generating virtually all available lateral force in all scenarios [5]. As a result, Fig. 6c shows that despite significantly

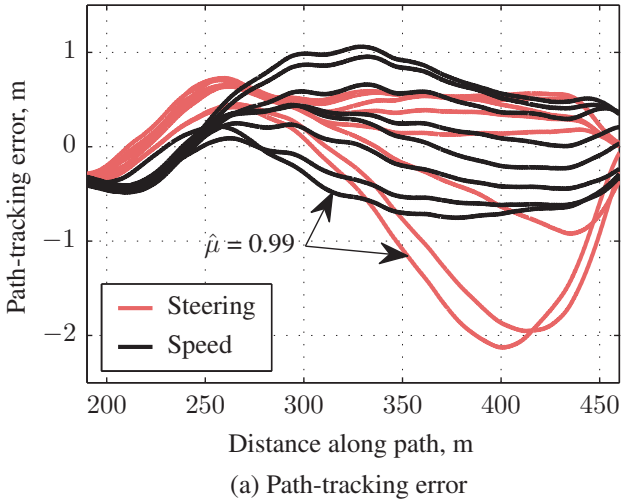

(a) Path-tracking error

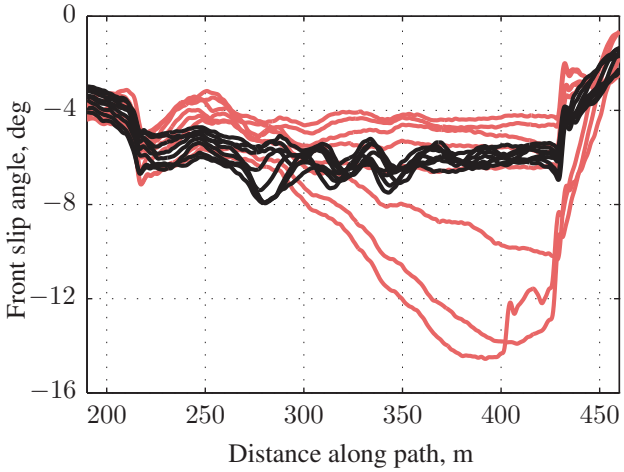

(b) Front slip angle

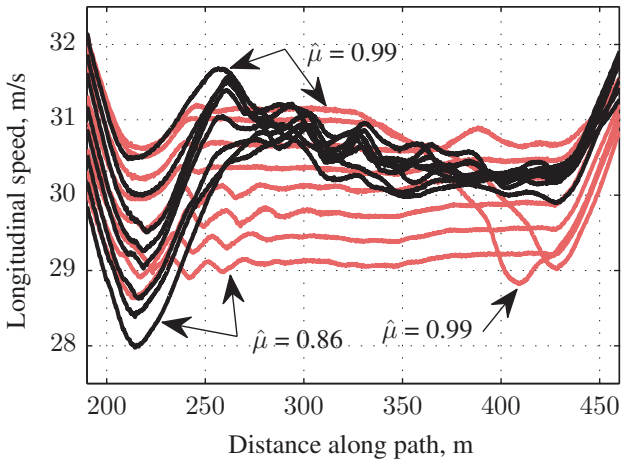

(c) Longitudinal speed

Figure 6: Experimental results of path tracking with steering or with speed feedback (new), for a range of friction estimates

different turn entry speeds, the vehicle ends up traveling at very similar longitudinal speeds with the different friction estimates – the maximum speed that the tires can support in this turn.

The two different control approaches not only show significant differences in their capability to track the desired path, they also show different results in the time it takes to complete the turn, in Fig. 8. When tire-road friction is underestimated, the conventional control approach is underutilizing the front tire-force potential, and it takes longer to complete the turn. For friction estimates at which the vehicle starts to slide not only is the longitudinal speed actually decreasing due to the additional steering drag, but the car is now also traveling more distance.

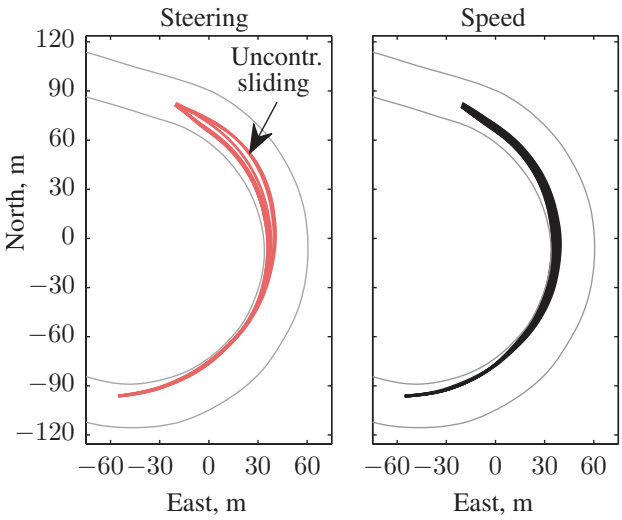

Figure 7: Collection of all driven trajectories with steering feedback (left) and speed feedback (right), with the distance from the track center line to the driven trajectories and the track boundaries magnified 3x to emphasize differences

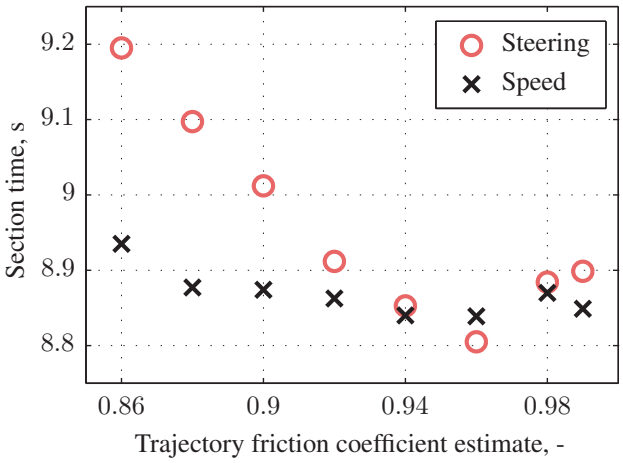

Figure 8: Section time from $s = 190$ m to $s = 460$ m

With speed feedback for path tracking, and the front tires operating close to their peak slip angle, the vehicle is still able to stay close to desired path when tire-road friction is overestimated. Under this framework the section time is relatively constant, and does not depend as strongly on the estimated friction, as virtually all available front lateral force is used in all scenarios.

7 DISCUSSION & FUTURE WORK

In the implementation of the speed controller it is assumed that the normal load at the front axle is constant. In reality, when the vehicle decelerates in response to a path-tracking error, longitudinal weight transfer to the front axle increases its lateral force capability. This, in addition to decelerating, will make the vehicle capable of driving an even tighter turn to return to the desired path. Vice versa, acceleration unloads the front axle and increases the vehicle's speed; both effects push the car onto a wider turn. Detailed analysis of the experiment results revealed that the weight transfer effect is a significant disturbance to the imposed path-tracking dynamics. Accounting for the effect of longitudinal weight transfer on the front axle lateral force would allow better tracking of the imposed path-tracking dynamics.

The imposed dynamics in (10) aim to drive the projected error at the COP to zero. It is known, however, that in general the steady-state heading error is nonzero [8], and hence the error at the COP would be nonzero in steady-state. By correcting (10) with a model for the steady-state heading error, the path-tracking performance could potentially be slightly improved.

In more experiments the framework proves to also work well in wet conditions. On snow and ice, when the tire-road friction coefficient can be as low as 5-10% compared to dry pavement, the framework is able to track the path, but at a slightly lower level of performance. Longitudinal force commands that modulate the longitudinal speed that in turn controls the path-tracking dynamics, which would be relatively small in dry conditions, have a larger (unmodeled) effect on the attainable front lateral force on low friction surfaces. This translates to a more significant disturbance to the path-tracking dynamics.

8 CONCLUSIONS

The analysis of a linearized single-track model illustrates that at the limit of tire-road friction steering becomes an ineffective input to control the path-tracking dynamics of an automated vehicle. A novel control framework is presented which employs speed feedback rather than steering feedback for path tracking, and operates the front tires near their peak slip angle to consistently utilize the full lateral force potential in cornering. Experimental results with a full-scale automated vehicle demonstrate how this new approach successfully controls the path-tracking dynamics at the limits of tire-road friction, and is able to robustly extract the full front tire-force potential even when there is significant uncertainty in the tire-road friction coefficient. In contrast, a conventional control architecture with only steering for path-tracking underutilizes the tire-force potential when the tire-road friction is underestimated, and the vehicle slides off the path uncontrollably when friction is overestimated. The results inspire completely new approaches to robust path-tracking control for automated vehicles.

REFERENCES

[1] G. M. Hoffmann, C. J. Tomlin, M. Montemerlo, and S. Thrun, "Autonomous automobile trajectory tracking for off-road driving: Controller design, experimental validation and racing," in *American Control Conference, 2007. ACC'07*, IEEE, 2007, pp. 2296–2301.

[2] K. Kritayakirana, "Autonomous vehicle control at the limits of handling," PhD thesis, Stanford University, 2012.

[3] J. Ziegler, P. Bender, M. Schreiber, H. Lategahn, T. Strauss, C. Stiller, T. Dang, U. Franke, N. Appenrodt, C. G. Keller, *et al.*, "Making bertha drive – an autonomous journey on a historic route," *IEEE Intelligent Transportation Systems Magazine*, vol. 6, no. 2, pp. 8–20, 2014.

[4] J. K. Subosits and J. C. Gerdes, "Autonomous vehicle control for emergency maneuvers: The effect of topography," in *2015 American Control Conference (ACC)*, IEEE, 2015, pp. 1405–1410.

[5] V. A. Laurense, J. Y. Goh, and J. C. Gerdes, "Path-tracking for autonomous vehicles at the limit of friction," in *American Control Conference (ACC), 2017*, IEEE, 2017, pp. 5586–5591.

[6] J. K. Subosits and J. C. Gerdes, "A synthetic input approach to slip angle based steering control for autonomous vehicles," in *American Control Conference (ACC), 2017*, IEEE, 2017, pp. 2297–2302.

[7] H. Pacejka, *Tyre and vehicle dynamics*, 3rd ed. Butterworth-Heinemann, 2012.

[8] N. R. Kapania and J. C. Gerdes, "An autonomous lane-keeping system for vehicle path tracking and stability at the limits of handling," in *Proceedings of the 12th International Symposium on Advanced Vehicle Control (AVEC)*, 2014, pp. 720–725.

[9] W. F. Milliken, D. L. Milliken, and M. Olley, *Chassis design: Principles and analysis*. Society of Automotive Engineers Warrendale, PA, 2002, vol. 400.